

## Diffraction study of the retained austenite content in TRIP steels

T. Gnäupel-Herold<sup>a,b,\*</sup>, A. Creuziger<sup>c,d</sup>

<sup>a</sup> NIST Center for Neutron Research, 100 Bureau Dr., Gaithersburg MD 20899-6102, USA

<sup>b</sup> University of Maryland, Department of Material Science and Engineering, College Park MD 20742-2142, USA

<sup>c</sup> NIST Metallurgy Division, 100 Bureau Dr., Gaithersburg MD 20899-8553, USA

<sup>d</sup> Kent State University, Kent, OH 44242, USA

### ARTICLE INFO

#### Article history:

Received 3 August 2010

Received in revised form 2 December 2010

Accepted 13 January 2011

Available online 19 January 2011

#### Keywords:

Austenite

Neutron diffraction

Texture

Steels

Deformation

### ABSTRACT

The results of a study of using neutron diffraction for determining the retained austenite content of TRIP steels are presented. The study covers a wide area of materials, deformation modes (uniaxial, biaxial and plane strain), strains, and the retained austenite content as a result of these variables. It was determined using basic principles of statistics that a minimum of two reflections ( $hkl$ ) for each phase is necessary to calculate a phase mass fraction and the associated standard deviation. Texture from processing the steel is the largest source of uncertainty. Through the method of complete orientation averaging described in this paper, the texture effect and with it the standard deviation of the austenite mass fraction can be substantially reduced, regardless of the type or severity of the texture.

© 2011 Elsevier B.V. All rights reserved.

### 1. Introduction

Steel typically may contain three different phases: austenite, ferrite, and martensite. The relative mass fractions of austenite and martensite have been of interest for a long time [1–14]. For new high performance steels such as transformation induced plasticity (TRIP) steels, accurate measurement of the austenite mass fraction is key. The measurement of the retained austenite content down to very low levels (less than 1% austenite) is a challenge for all suitable methods, and diffraction is no exception. However, with the established theoretical principles of diffraction, accurately measured composition, and suitable signal to noise ratios the actual detection limit could be significantly lower than 1%. The achievable accuracy is limited by several factors, with texture being the most significant.

So far the difficulties associated with texture, and there is virtually no steel without texture, have been dealt with in a heuristic manner by issuing recommendations to use procedures for weakly textured samples [1] or for untextured samples [2]. In [1] Jatzcak focuses entirely on X-ray diffraction and recommendations are made for dealing with texture using a scheme of partial orienta-

tion averaging of multiple reflections through rotation and limited tilt but without regard to the different statistical weight of  $\psi$ -tilts and the effect of the missing tilt range. The error analysis presented in [1] uses either the counting statistics or repeated measurements with remounting of the same sample. Both methods have serious limitations because they largely miss the texture effect and they tend to produce unrealistically small uncertainties. To our knowledge, there has been no systematic study of the effects of texture on the calculation of retained austenite mass fraction.

Good agreement in the measured retained austenite content was achieved in an X-ray diffraction round-robin [3]. However, the standard reference samples used there have since been withdrawn. In a recent round robin, different characterization techniques were used to measure the retained austenite in TRIP steel [4,5]. There was significant scatter in the mass fractions calculated, both between the different methods used and between the same methods, indicating there can be a significant bias error associated with different methods or labs. At the same time, the standard deviations given by each measurement were unrealistically low, thus indicating a real lack of consistency in calculating both of mass fractions and their uncertainties.

This paper focuses on the use of neutrons and schemes for orientation averaging to measure austenite mass fractions on TRIP steels. Neutron diffraction has many advantages over some of the other techniques mentioned and employed in [4]; for example, each measurement takes place over volumes of 10–100 mm<sup>3</sup> and the methods for determining phases by diffraction methods are well developed. In this paper, a suitable orientation averaging proce-

\* Corresponding author. NIST Center for Neutron Research, 100 Bureau Dr. stop 6102, Gaithersburg, MD 20899-6102, USA, Tel.: +1 301 975 5380; fax: +1 301 921 9847.

E-mail addresses: [tg-h@nist.gov](mailto:tg-h@nist.gov) (T. Gnäupel-Herold), [adam.creuziger@nist.gov](mailto:adam.creuziger@nist.gov) (A. Creuziger).

ture that permits the effect of texture to be largely suppressed is discussed. These methods allow for precise measurement of the austenite mass fraction and the standard deviations.

## 2. Experimental

### 2.1. Diffraction method

The estimation of the volume fractions in a polycrystalline specimen containing different phases and with a random grain orientation distribution by means of diffraction is based on the relationship of the calculated integrated intensity  $R_{hkl}^{(i)}$  of a diffraction line ( $hkl$ ) for phase  $i$  and the volume fraction  $V_i$  of that phase in the specimen. The expression used here can be written as [6–8,15]

$$R_{hkl}^{(i)} = KV_i \frac{j\lambda^3 F_{hkl}^2}{v_i^2 \sin \theta \sin 2\theta} e^{-B \frac{\sin^2 \theta}{\lambda^2}} A_{hkl} \quad (1)$$

where  $K$ : constant specific for the experiment;  $j$ : multiplicity of the plane ( $hkl$ );  $\lambda$ : wavelength;  $F_{hkl}^2$ : structure factor of the plane ( $hkl$ );  $v_i$ : unit cell volume of phase  $i$ ;  $B$ : Debye–Waller factor;  $\theta$ : Bragg angle;  $A_{hkl}$ : absorption factor. The absorption factor depends on the linear absorption coefficient and the specimen shape. It was found to be negligible in this investigation. The theoretical structure factors  $F_{hkl}$  were calculated using the widely available Powder Cell [16] program; for  $B$  the value 0.35 was used as quoted in [17]. If all intensities are measured on the same equipment, and under the same conditions, the term  $K$  may be dropped, as it will for subsequent discussion.

The steel specimens investigated here contain ferrite ( $\alpha$ ), retained austenite ( $\gamma$ ) and martensite ( $m$ ). Bainite, which is typically encountered in TRIP steels, is a particular structure of ferrite with austenite laths. Due to the alloying in TRIP steels, excess carbon is partitioned to the austenite instead of forming cementites as in conventional bainite. The martensite peaks cannot be resolved from the ferrite peaks [18]; thus, only the austenite ( $\gamma$ ) and the ( $\alpha + m$ ) volume fractions can be determined. The austenite mass fraction value is not affected by the presence of the martensite phase because the sum of the structure factors of overlapped martensite and ferrite peaks is practically identical to that of the ferrite peak with the martensite replaced by ferrite. Also, the austenite peaks are unaffected by martensite. As these phases are the only constituents in a TRIP steel, the volume fractions of each phase must add to one ( $V_\alpha + V_m + V_\gamma = 1$ ) and the volume fraction of the austenite phase can be correlated to the measured integrated intensities  $I_\gamma^{(\gamma)}$  and  $I_\gamma^{(\alpha+m)}$  by

$$V_\gamma = \frac{\left( \frac{1}{n} \sum_{l=1}^n \frac{I_l^{(\gamma)}}{R_l^{(\gamma)}} \right)}{\left( \frac{1}{m} \sum_{l=1}^m \frac{I_l^{(\alpha+m)}}{R_l^{(\alpha+m)}} + \frac{1}{n} \sum_{l=1}^n \frac{I_l^{(\gamma)}}{R_l^{(\gamma)}} \right)} = \frac{\bar{I}(\gamma)}{\bar{I}(\gamma) + \bar{I}(\alpha+m)} \quad (2)$$

where ( $n$ ) and ( $m$ ) are the number of diffraction peaks for each phase. The mass fraction is obtained from the densities ( $\rho$ ) of each phase:

$$f_\gamma = \frac{(V_\gamma \rho_\gamma)}{(V_\gamma \rho_\gamma + V_{\alpha+m} \rho_{\alpha+m})} \quad (3)$$

Eq. (2) contains averages of integrated intensities normalized by theoretical intensities. It is reasonable to use a longer counting time for weak reflections, thus requiring time normalization as well. In order to allow for the statistical nature of the intensities in Eq. (2) one must consider the effects of individual standard deviations as well as the averages calculated in Eq. (2). The standard deviation

of the measured integrated intensity of a peak ( $\sigma_p$ ) is derived from the counting statistics through:

$$\sigma_p = \sqrt{\sigma_T^2 + \sigma_B^2} \quad (4)$$

with  $\sigma_T = 0.675 \sqrt{I_T}$  as standard deviation of the total intensity  $I_T$  of the peak including background, and  $\sigma_B = 0.675 \sqrt{I_B}$  as standard deviation of the background [19]. In principle, through sufficiently long counting times  $\sigma_p$  could be reduced to arbitrary small values and, through error propagation in Eq. (2), a similarly small standard deviation could be achieved for  $V_\gamma$ . In reality this is not the case. First, the averages in Eq. (2) need to be modified to allow for the different individual  $\sigma_p$  as weights:

$$\bar{I} = \frac{\left( \sum_{l=1}^n I_l / (R_l \sigma_l^2) \right)}{\sum_{l=1}^n 1/\sigma_l^2} \quad (5)$$

Second, the normalized intensities  $I/R$  for each phase imply that they are equal after the various normalizations for structure factor, multiplicity, polarization, etc. This is usually not fulfilled because of counting statistics, texture, imperfect diffraction geometry, specimen shape and insufficient knowledge of specimen material parameters such as the precise elemental distribution of constituent elements over phases and crystallographic sites. It is assumed that all these influences combined act as one individual uncertainty for each reflection. Thus, the variance of the average normalized intensities is

$$\sigma_{\bar{I}}^2 = \frac{1}{n-1} \sum_{l=1}^n (\bar{I} - I_l)^2 \quad (6)$$

The counting statistics still plays a role for  $\sigma_{\bar{I}}^2$  as a contributor to the scatter. Note that the factor ( $n-1$ ) allows for the fact that  $\bar{I}$  was determined from the average of the  $I_l$ . The standard deviation of the volume fraction becomes

$$\begin{aligned} \sigma_{V_\gamma} &= \sqrt{\sigma_{\bar{I}(\gamma)}^2 \left( \frac{\partial V_\gamma}{\partial \bar{I}(\gamma)} \right)^2 + \sigma_{\bar{I}(\alpha+m)}^2 \left( \frac{\partial V_\gamma}{\partial \bar{I}(\alpha+m)} \right)^2} \\ &= \sqrt{\frac{\sigma_{\bar{I}(\gamma)}^2 (\bar{I}(\alpha+m))^2 + \sigma_{\bar{I}(\alpha+m)}^2 (\bar{I}(\gamma))^2}{(\bar{I}(\gamma) + \bar{I}(\alpha+m))^4}} \end{aligned} \quad (7)$$

which can be converted to a mass fraction using the known densities. From Eqs. (5), (6), (7) it follows that the measurement of only one single peak for austenite and ferrite does not allow the proper calculation of a mass fraction or its standard deviation. From equation (6) the factor  $1/(n-1)$  requires at least two peaks. Physically speaking, at least a second peak is necessary to compare the normalized intensities and to calculate an uncertainty; with only one peak one has to assume an ideally random sample, a condition that is rarely fulfilled. By having at least a second reflection available (more are desirable) one has in essence an internal measure of scatter through the differences in  $I/R$  for a particular phase in Eq. (2).

Eq. (2) is also the basis for the standard procedure in [2] which explicitly states that specimens should be texture free. It is well known that in steels some preferred grain orientation is always present, thus making the intensity dependent on the specimen orientation. If left uncorrected, textured samples produce a very large scatter in diffraction-based estimates of phase fractions. A correction can be performed in two ways: (1) By averaging over

**Table 1**  
Chemical composition (wt %) of the TRIP samples investigated.

Sample	Material	C	Mn	Al	Si	Thickness (mm)
A	TRIP 700	0.23	1.49	2.02	0.04	1.0
B	TRIP 590	0.10	1.48	0.059	1.19	1.6
C	TRIP 780	0.16	2.07	2.04	0.03	1.0

sufficiently many, and suitably different specimen orientations and (2), by using the orientation distribution function (ODF) for the calculation of the integrated intensity with texture effect.

For the purpose of volume/mass fraction determination the first approach, here called complete orientation averaging, is preferable because it requires far less measurement time. In that case, a summation of peaks measured at different specimen orientations is performed and the average intensity of the peak used to determine the phase fraction. Method (2) requires a known ODF from which one can calculate the multiples of random density numbers (*m.r.d.*) for the combinations of (*hkl*) and specimen orientations used in the measurement.

Method (1) is used extensively as the basis for the neutron diffraction texture measurements where individual measurements are taken for ( $\varphi\psi$ ) values obtained by a reverse equal-area projection from a plane onto the pole sphere. The locations on the plane are the central points of equal-sized hexagons, which, through area-preservation of the projection, yield directions with nearly constant angular distance between neighboring points [20,21]. This is realized in the meshes shown in Fig. 1.

The orientation mesh in Fig. 1 left represents a nearly ideal case: how well the orientation average is achieved depends only on the angular width of intensity poles with respect to the spacing of orientations. When averaging the intensities of different reflections (*hkl*) this effect is a contributor to the variance in Eq. (6). With the complete orientation averaging each sample orientation has equal weight; a non-equidistant spacing could be used instead but would require the introduction of weight factors to correct for over/under-representation of some orientations.

## 2.2. Samples

Three different grades of commercially produced TRIP steels were investigated: TRIP590, TRIP700 and TRIP780. The numbers following TRIP indicate the nominal ultimate tensile strength in MPa. These samples are sheet stock; their chemical compositions and as received thickness are given in Table 1.

The deformation modes included uniaxial deformation parallel to the rolling direction (RD), uniaxial deformation parallel to the transverse direction (TD), in plane-strain deformation ( $\varepsilon_2 = 0$ ) with the straining direction parallel to the rolling direction (PS-RD) plane-strain deformation parallel to the transverse direction (PS-TD), and balanced biaxial deformation (BB) ( $\varepsilon_1 = \varepsilon_2$ ). TRIP700 was investigated only in the undeformed state. TRIP590 samples were measured in the undeformed state and at nominal deformations of 2%, 5%, 10%, 15%, 20% and 25% engineering strain with the exception of a PS-TD sample that failed before reaching 25% strain. TRIP780 samples were measured in the undeformed state and at nominal deformations of 2%, 5% and 10% engineering strain. The equipment used to deform the samples is described in more detail in [22]. In order to create sufficient scattering volume, reduce data acquisition times and produce an equal-axial sample shape, the sheet material was sheared into small plates and glued together into cubes (6 mm × 6 mm × 6 mm) while maintaining the plate orientations. The densities used here were obtained by Rietveld analysis of neutron diffraction patterns measured on the undeformed samples B ( $\rho_{\alpha+m} = (7.749 \pm 0.002) \text{ g/cm}^3$  and  $\rho_{\gamma} = (7.765 \pm 0.018) \text{ g/cm}^3$ ) and

C ( $\rho_{\alpha+m} = (7.591 \pm 0.004) \text{ g/cm}^3$  and  $\rho_{\gamma} = (7.668 \pm 0.016) \text{ g/cm}^3$ ). For sample A (TRIP700), the values for sample C were used because of the similar composition.

## 2.3. Diffraction measurements

The integrated intensities, averaged over all orientations were determined from the fit of a gaussian with linear background function. Values of the standard deviation ( $\sigma$ ) were obtained from the respective standard deviation of the peak height and the width.

The neutron measurements of individual, non-overlapping peaks were done at the BT8 residual stress diffractometer at CNCR using a full-circle Euler cradle for specimen orientation [23]. The steel samples are fully bathed in the neutron beam at all orientations. Because of the low attenuation of neutrons, the entire sample contributes almost uniformly to the diffracted beam. Absorption effects were found to be negligible for the specimens used in this work.

A total of six reflections – three for austenite, three for ferrite – were used for mass fraction estimation. A Si (3 1 1) monochromator produced a wavelength of  $\lambda = 0.1637 \text{ nm}$  without  $\lambda/2$  contamination, thus putting the three austenite reflections: A200, A220 and A311 at values of  $2\theta$  of ( $54^\circ$ ,  $79^\circ$ ,  $96^\circ$ ) and for ferrite F200, F211 and F220 at values ( $69^\circ$ ,  $88^\circ$ ,  $107^\circ$ ), within the available  $2\theta$ -range of  $45^\circ$ – $110^\circ$ . The composition given in Table 1 was used to calculate the structure factors.

The method of complete orientation averaging represents the measurement of a complete pole figure, albeit not necessarily at counting times or  $\varphi\psi$ -mesh resolution required to calculate the ODF. A minimum of 127 orientations in  $\varphi\psi$ -mesh resolution was used for the calculation of retained austenite content (see Fig. 1). Control measurements were done using five different powders (Fe, Mo, Cu, Al, Ni). Orientation averaging was not carried out on the control powder measurements because the cylindrical shape of the sample container did not allow that a constant volume of sample material be illuminated by the beam at all orientations.

Selected X-ray measurements were performed using filtered Mo-K $\alpha$  radiation in a partial averaging scheme up to  $45^\circ$   $\psi$ -tilt (see pictograms in Fig. 3, right).

## 3. Results

The determination of mass fractions based on the comparison of orientation averaged peaks as laid out in Eq. (1)–(7) is largely limited by the signal/noise ratio which decreases with decreasing austenite content. However, all austenite peaks were well behaved, and no constraints for the peak position or the width were used. The ferrite peak shapes were symmetric without indication of martensite peaks.

Measurements of peaks from the various control powder materials were used to demonstrate the effect of insufficient orientation averaging even for samples deemed to be random. This is shown in the normalized intensities vs.  $2\theta$  (Fig. 2). As mentioned, sample container geometry precluded using orientation averaging while measuring the powder materials. For the random orientation assumption, the normalized intensity should not depend on  $2\theta$ . However, the relative differences up to 30% in the normalized intensities in Fig. 2, left, are most likely caused by texture from the settling of the powder particles. Thus, it provides an excellent illustration of the difficulties that can arise from the assumption of random grain orientation even for powder samples that are typically assumed to be untextured. The normalized intensities are shown only as a representative example for two TRIP590 samples, one sample as undeformed and one sample strained to 20% in the PS-TD strain state in Fig. 2, right. The

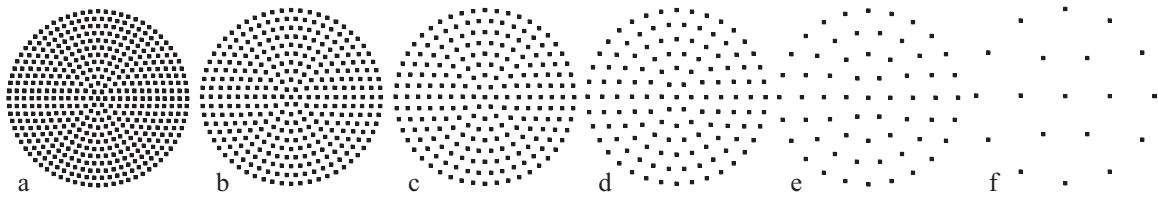


**Fig. 1.** Specimen orientations in spherical polar coordinates ( $\varphi/\psi$ ) plotted in equal-area projection. The circles represent the azimuth angle  $\varphi$  (sample rotation); the radial distance is the tilt angle  $\psi$ . At the center  $\psi$  is zero and the  $\varphi$ -axis is parallel to the bisector of incident and diffracted beam (scattering vector). The mesh resolutions are (left to right, with  $\Delta\varphi_{\psi=90^\circ}$  in brackets) a: 469( $5^\circ$ ), b: 331( $6^\circ$ ), c: 217( $7.5^\circ$ ), d: 127( $10^\circ$ ), e: 61( $15^\circ$ ), f: 19( $30^\circ$ ).

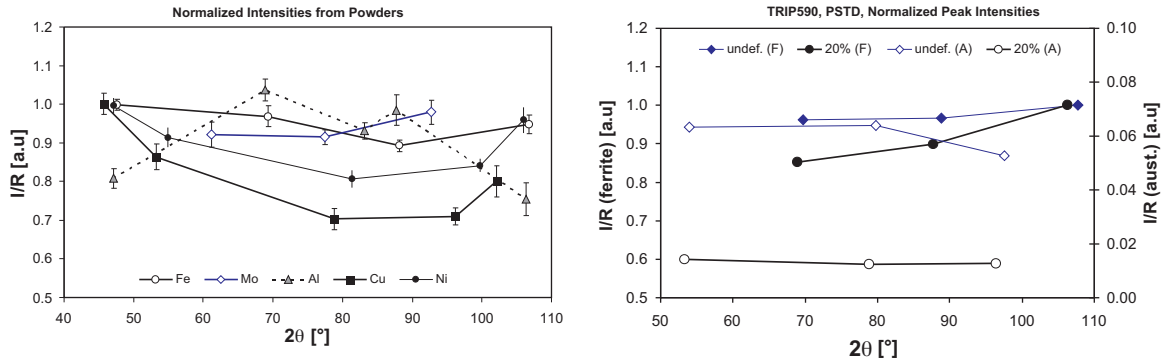


**Fig. 2.** Left: Normalized intensities ( $I/R$ ) for peaks from various powders. The following peaks were measured: Cu, Ni: (111), (200), (220), (311), (222); Al: (200), (220), (311), (222), (400); Fe: (110), (200), (211), (220); Mo: (200), (211), (220). Right: Normalized integrated intensities for TRIP 590, undeformed and 20% strain PS-TD with ferrite peaks (200), (211), (220) and austenite peaks (200), (220) and (311). In the right graph the  $\sigma$ -values are of the size of the markers or smaller.

$I/R(2\theta)$  for all other samples displayed a very similar behavior.

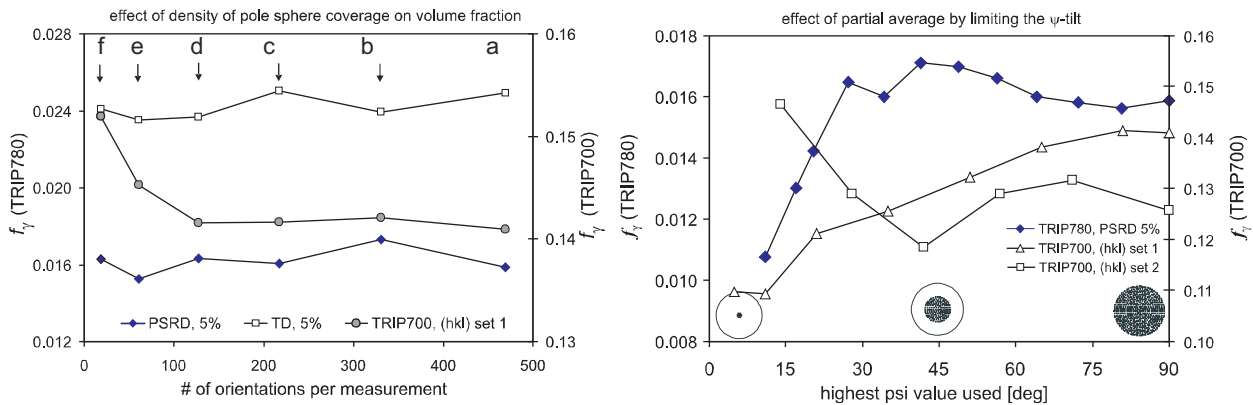
For the TRIP steel the  $I/R$  both for ferrite and austenite have small slopes over  $2\theta$ . Through measurements with different mesh resolutions in complete and partial orientation averaging it was found that imperfect orientation averaging together with the particular combination of reflections ( $hkl$ ) used here could cause this behavior. However, one should note that overall the differences between normalized intensities over  $2\theta$  are much smaller ( $\max \times 7\%$ ) for the TRIP sample with complete orientation averaging than for the powder samples ( $\max \pm 17\%$ ) without comparable orientation averaging.

Instead of a complete orientation average with varying point density one can also consider a partial average limited by tilt. Such a case arises if the tilt angle ( $\psi$ ) range is restricted as it is the case in X-ray diffraction. These data were created by partitioning of existing data sets from complete orientation averaging. At  $\psi \approx 0$  one has

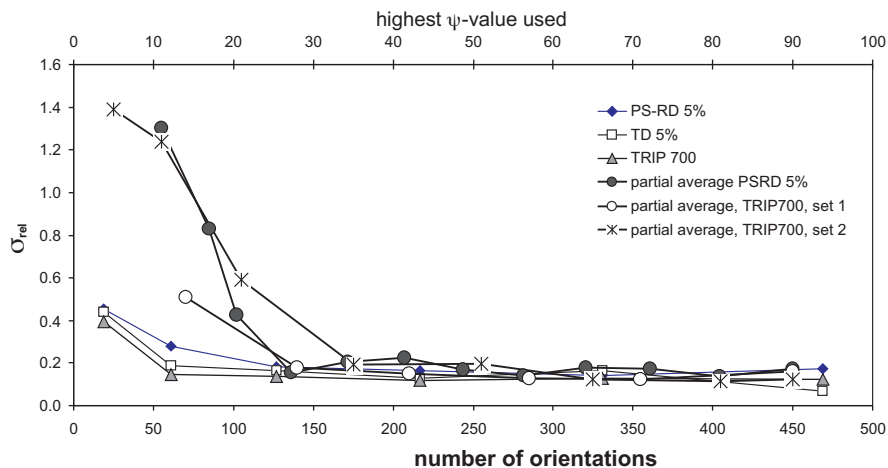
the case of a  $\theta$ - $2\theta$  scan at one orientation. Consequently, the mass fractions derived from these measured intensities deviate significantly from the result obtained with complete orientation average. As larger  $\psi$  values are included, the calculated values converge again. However the trends prior to the convergence are not consistent between different samples, showing the need to measure at higher  $\psi$  angles to improve accuracy.

Fig. 3 demonstrates the effect of the number of orientations in the mass fraction value. As the number of orientations increase there is convergence in the mass fraction measurement. The mass fractions do not show a strong dependence on the number of orientations beyond 100 orientations measured.

The effects of  $\varphi/\psi$ -mesh densities (see Fig. 1) or limited tilt capability are clearly reflected in the dependence of relative standard deviation shown in Fig. 4. Values for  $\sigma_{rel}$  increase steeply below 100 orientations per measurement (complete averaging scheme) or for averaging in a  $\psi$ -range less than  $30^\circ$  from the sample nor-



**Fig. 3.** Effect of different numbers of individual orientations on the calculated austenite mass fraction. Left: complete orientation averaging with different mesh densities with letters a–f referring to the meshes in Fig. 1. Right: Partial orientation averaging with limited  $\psi$ -tilt. The grey area in the pictograms indicate the tilt range used with the x-axis as the  $\psi$  cut-off. A value of  $\psi = 0$  would be the equivalent of a  $\theta$ - $2\theta$  scan with only one contributing orientation per reflection. TRIP 700 set 1 refers to A(220), A(311), A(420) and F(211), F(220), F(321). Set 2 refers to A(200), A(220), A(311) and F(200), F(220).



**Fig. 4.** Relative standard deviations for the complete averaging scheme (bottom axis) and for partial averaging in limited  $\psi$ -tilt (top axis). Low values on the top axis mean fewer orientations just as on the bottom axis.

mal. Beyond that, the relative standard deviation values are stable at 10–20%.

Larger fluctuations in the calculated value of the mass fraction are observed if different combinations of orientation averaged reflections ( $hkl$ ) are used. Fig. 5 illustrates very effectively the reason why mass fraction calculations based on single reflections are unreliable. First, the calculation of the standard deviation is not possible with Eq. (6), and second, the effects of insufficient orientation average are amplified leading to relative minimum/maximum differences of up to 50% in the mass fraction. The standard deviations  $\sigma$  calculated from the counting statistics (1A/1F combinations) are too small as evident from the comparison with the  $\sigma$  values for  $f_\gamma$  from combinations of multiple reflections (Fig. 5, left). Due to instrumental restrictions the pool of simultaneously accessible reflections is restricted to ferrite (110), (200), (211), (220) with austenite (111), (200), (220), (311) and (222). However, the austenite (111) and (222) reflections are difficult to measure for small mass fractions due to their low multiplicity and some overlap with neighboring ferrite reflections. Therefore the undeformed TRIP700, which had the largest austenite mass fraction, was chosen to investigate a large number of different combinations of reflections (Fig. 5, right).

The 2A/2F combination requires fewer measurements than 3A/3F or 5A/4F but comes at the expense of a larger  $\sigma$  expressed through the larger scatter than 3A/3F. This uncertainty is not related to the counting statistics but stems from the previously discussed effects of insufficient orientation average and limited knowledge of the phase specific chemical composition. The 5A/4F combination represents the maximum available data with a total of 2979 individual intensity measurements but it does not come with a significant reduction in  $\sigma$ . In effect, the relative standard deviation for the data in Fig. 4 has a lower limit of approximately 10%. A similar threshold for  $\sigma$  exists for TRIP590 and TRIP780, both of which have much lower contents of retained austenite.

The mass fractions for different deformation regimes and strains are shown in Fig. 6 for TRIP780 and TRIP590. They are plotted in terms of effective strain, which is the Von Mises average of the true strains:

$$\varepsilon_{eff} = \frac{\sqrt{2}}{3} [(\varepsilon_{11} - \varepsilon_{22})^2 + (\varepsilon_{22} - \varepsilon_{33})^2 + (\varepsilon_{33} - \varepsilon_{11})^2]^{\frac{1}{2}} \quad (8)$$

This allows different strain states to be compared directly. The austenite mass fractions measured follow a similar curve for all three strain modes explored, similar to results shown in [5].

For the purpose of comparison selected X-ray measurements were performed on three undeformed samples with results shown in Table 2. The austenite weight fractions are comparable to the neutron results when using the X-ray standard deviations. However, this is not always the case when considering the much smaller standard deviations from neutron diffraction measurements. Two main reasons for this discrepancy were identified: the generally low X-ray signal/noise ratio ( $\leq 1/10$ ) and the “missing orientations” from the  $\psi$ -tilt limited to values  $\leq 45^\circ$ . The wider effects of the averaging scheme in connection with different textures on weight fractions derived from X-ray diffraction is currently under investigation.

#### 4. Discussion

The values of retained austenite measured for the TRIP steels investigated here are comparable to the range of retained austenite measured by Jacques et al. [4] as part of round robin. As noted previously, the round robin data shows a great deal of scatter, and ranges from 2% to 36% austenite. While the TRIP 590 and TRIP 780 steels are on the low end of this range, they are commercially produced alloys. The TRIP 700 steel falls into the middle of the range of retained austenite with a value of 15%. From the composition data, there does not seem to be a strong effect from alloying alone, the thermo-mechanical processing plays a strong role in the final austenite value. Similarly, comparing the retained austenite value alone of the TRIP steels does not give an indication to the strength and ductility of the different steels.

Comparing the retained austenite as a function of applied strain and strain state in Fig. 6 shows some differences and commonality between the TRIP 590 and TRIP 780 alloys. Neither alloy shows a strong effect from stress triaxiality, as predicted previously [5]. In both materials the lowest retained austenite value occurs near failure in the balanced biaxial strain state, and appears to reach

**Table 2**

Austenite mass fractions for three different TRIP steels (undeformed) as obtained from complete orientation average (neutron diffraction) and partial average/X-ray diffraction.

Sample	Wt. fraction (X-ray)	$\sigma$	Wt. fraction (neutron)	$\sigma$
TRIP 700	0.156	0.038	0.135	0.016
TRIP 590, undeformed	0.053	0.045	0.058	0.006
TRIP 780, undeformed	0.039	0.032	0.051	0.003

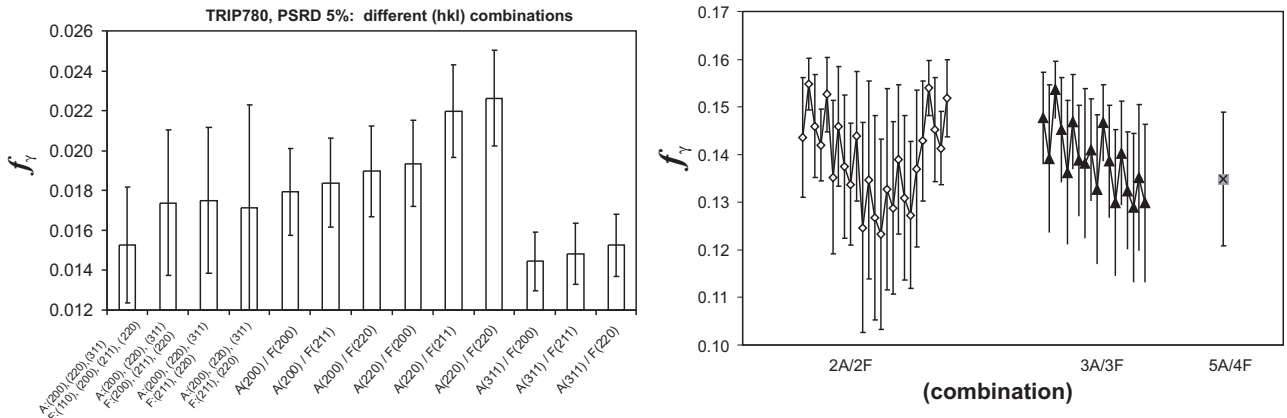


**Fig. 5.** Effect of  $(hkl)$ -combinations on the mass fraction  $f_\gamma$ . Left: TRIP 780 sample strained in PS-RD 5%. Right: TRIP 700, undeformed. 2A/2F and 3A/3F use different combinations of  $(hkl)$  out of 5A/4F (Austenite: (111), (200), (220), (311), (222) with Ferrite: (110), (200), (211), (220)). The  $\sigma$ -values for combinations of single reflections are calculated from the counting statistics. Each reflection was measured with 331 orientations.

a plateau value before reaching failure. In contrast the uniaxial deformation samples follow the plane strain and balanced biaxial for the TRIP 590 samples, while in the TRIP 780 alloy there is more retained austenite for both uniaxial samples, with the TD oriented sample having a higher austenite value for higher levels of strain. This will be investigated further in the future, but may be due to differences transformation potential due to crystallographic orientation discussed in [24].

The method of complete orientation averaging provides a precise method for measuring the retained austenite mass fraction. With this method, the retained austenite mass fractions can be measured to levels less than 1% with standard deviations on the order of 10%. This overall precision of 10% (Fig. 4) was found for the entire range of austenite mass fractions (from 0.01 to 0.14), even if significantly more orientations contribute to the average.

It is difficult to compare this precision with other published results, mostly due to the lack of detail about the error estimation procedures. The two methods given in [1] should be seen in a critical light because both methods do not take texture into account, and, compared with the results presented here, both may underestimate  $\sigma$  by a significant amount. For example, for all samples where  $\sigma$  is estimated solely based on the count rate, the standard deviation is over 10 times smaller than the values given here from Eq. (7). Such a low value clearly does not reflect the observed scatter.

The results presented here on the role of texture and orientation averaging can offer some explanation of the large variability in the X-ray results of the round-robin in [4]. The results listed in the round-robin presumably follow the SAE [1] or ASTM [2] guide-

lines, while no details are given. As shown in this paper an austenite mass fraction  $f_\gamma$  derived from a partial orientation average is subject to a large relative deviation. A necessary condition to obtain a meaningful value for  $f_\gamma$  – which includes a meaningful uncertainty – is that a minimum of two diffraction lines from both ferrite and austenite are needed to accurately determine  $f_\gamma$ . Neither of these criteria are stated in the ASTM standard [2] and the requirement on the tilt axis is not explicitly stated in the SAE publication by Jatzcak [1]. The statement in [1] that if tilt and rotation are performed, only one line pair is needed is also incorrect because no meaningful uncertainty can be given for  $f_\gamma$ . The assumption of a random orientation distribution is hard to justify, given the scatter of intensities of powder samples investigated here. The latter result in particular (Fig. 2) demonstrates that at least for the purpose of mass fraction determinations a sample cannot be assumed to have no or negligible texture. The recommendation of four  $(hkl)$  pairs if the sample is not rotated or tilted is also insufficient because each additional reflection  $(hkl)$  improves the average only by the multiplicity of that particular  $(hkl)$ .

The retained austenite content determined from partial averaging schemes such as X-ray diffraction is susceptible to ‘missing’ orientations from limited  $\psi$ -tilt (Fig. 3, left). Complete orientation averaging schemes require a minimum density of orientations in order to yield stable results. That number depends on the type and strength of the underlying texture. Fig. 3 indicates that number to be >100 for the samples investigated here. This underscores some of the advantages of neutron diffraction: superior grain statistics ( $10^3$  more contributing grains than X-ray diffraction), and easier

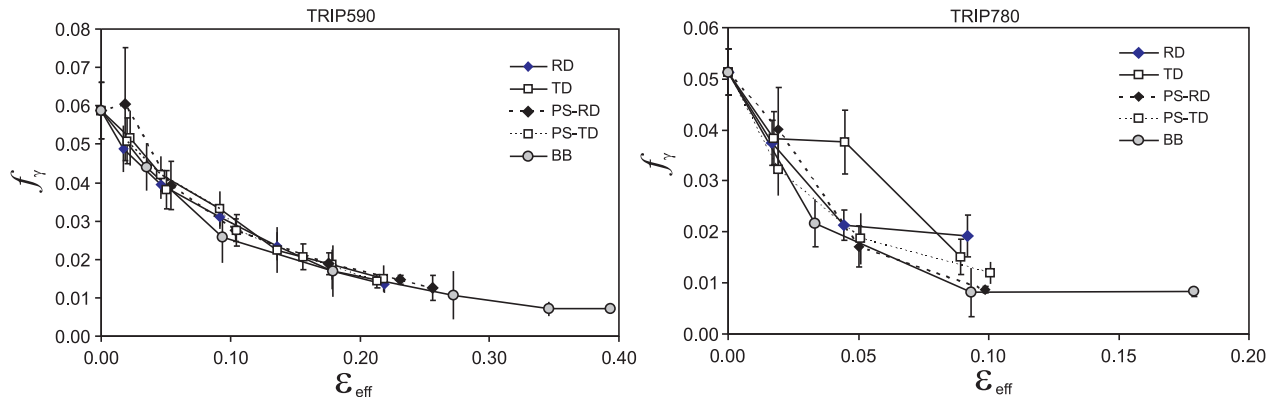


**Fig. 6.** Austenite mass fractions  $f_\gamma$  for TRIP 590 (left) and TRIP 780 (right). The deformation modes are uniaxial in RD and TD, in plane-strain deformation ( $\epsilon_2 = 0$ ) parallel to RD and TD (labeled as PS-RD and PS-TD), and balanced biaxial deformation (BB) ( $\epsilon_1 = \epsilon_2$ ).

complete orientation averaging. In comparison, X-ray diffraction is limited by its low penetration and tilt angle restrictions.

## 5. Conclusions

A method of austenite mass fraction measurement, termed complete orientation averaging has been demonstrated. If an unknown texture is present then averaging over sufficiently many (over 100) specimen orientations is necessary in order to reduce the influence of texture. Additionally, the measurement of at least two peaks for each phase are necessary to calculate the standard deviation and thus a minimum requirement for reliable measurement of the austenite mass fraction. Within the range of results obtained here the relative accuracy of neutron diffraction with complete orientation averaging is remarkably stable, and even austenite mass fractions down to values <0.01 were determined with good precision ( $\sigma_{\text{rel}} = 10\%$ ).

## 6. Disclaimer

Certain commercial firms and trade names are identified in this report in order to specify aspects of the experimental procedure adequately. Such identification is not intended to imply recommendation or endorsement by the National Institute of Standards and Technology, nor is it intended to imply that the materials or equipment identified are necessarily the best available for the purpose.

## References

- [1] C.F. Jaczak, J.A. Larson, S.W. Shin, SAE Special Publication 453 Retained Austenite and its Measurements by X-ray Diffraction, 1980.
- [2] ASTM E975-00, Standard Practice for X-Ray Determination of Retained Austenite in Steel with Near Random Crystallographic Orientation, vol. 03.01, ASTM International, W. Conshohocken, PA, 2003.
- [3] R.W. Hinton, J. Testing Eval. 15 (1987) 95–100.
- [4] P.J. Jacques, S. Allain, O. Bouáziz, A. De, A.-F. Gourgues, B.M. Hance, Y. Houbaert, J. Huang, A. Iza-Mendia, S.E. Kruger, M. Radu, L. Samek, J. Speer, L. Zhao, S. van der Zwaag, Mater. Sci. Technol. 25 (2009) 567–574.
- [5] P.J. Jacques, Q. Furnémont, F. Lani, T. Pardoën, F. Delannay, Acta Mater. 55 (2007) 3681–3693.
- [6] J. Zrník, O. Muransky, P. Lukas, P. Sittner, Z. Novy, Mater. Sci. Forum 502 (2005) 339–344.
- [7] M. Cermansky, J. Cermak, N. Zarubova, P. Wolf, J. Mater. Sci. 31 (1996) 995–1004.
- [8] A.K. De, D.C. Murdock, M.C. Mataya, J.G. Speer, D.K. Matlock, Scripta Mater. 50 (2004) 1445–1449.
- [9] S. Cheng, X.L. Wang, Z. Feng, B. Clausen, H. Choo, P.K. Liaw, Metall. Mater. Trans. 39A (2008) 3105–3112.
- [10] J.M. Pardal, S.S.M. Tavares, M.P. Cindra-Fonseca, J. Mater. Sci. 41 (2006) 2301–2307.
- [11] R.W. Cheary, Y. Ma-Sorrell, J. Mater. Sci. 35 (2000) 1105–1113.
- [12] S.H. Magner, R.J. De Angelis, W.N. Weins, J.D. Makinson, Adv. X-ray Anal. 45 (2002) 92–97.
- [13] B.S. Seong, E.J. Shin, Y.S. Han, C.H. Lee, Y.J. Kim, S.J. Kim, Physica B 350 (2004) e467–e469.
- [14] P.J. Jacques, Q. Furnémont, S. Godet, T. Pardoën, K.T. Conlon, F. Delannay, Phil. Mag. 86 (16) (2006) 2371–2392.
- [15] G.E. Bacon, Neutron Diffraction, Oxford University Press, London, 1962.
- [16] W. Kraus, G. Nolze, J. Appl. Cryst. 29 (1996) 301–303.
- [17] S.K. Mohanlal, J. Phys. C 12 (1979) L651–L653.
- [18] R. Fillipone, J. Root, P.J. Jacques, S. Yue, ISIJ Int. 42 (2002) 304–309.
- [19] H.P. Klug, L.E. Alexander, X-ray Diffraction Procedures, Wiley & Sons, New York, 1954.
- [20] S. Matthies, H.-R. Wenk, Phys. Stat. Sol. A 133 (1992) 253–257.
- [21] K. Helming, Texturapproximation Durch Modellkomponenten, Cuvillier, Göttingen, 1996.
- [22] T. Foecke, M.A. Iadicola, A. Lin, S. Banovic, Metall. Mater. Trans. A 38A (2007) 306–313.
- [23] P.C. Brand, H.J. Prask, T. Gnaeupel-Herold, Physica B 241–243 (1997) 1244–1245.
- [24] A. Creuziger, T. Foecke, Acta Materialia 58 (2010) 85–91.